Nanoscale

PAPER

View Article Online
View Journal | View Issue

Cite this: *Nanoscale*, 2014, **6**, 1879

Graphene oxide exhibits broad-spectrum antimicrobial activity against bacterial phytopathogens and fungal conidia by intertwining and membrane perturbation†

Juanni Chen, Hui Peng, Xiuping Wang, Feng Shao, Zhaodong Yuan and Heyou Han*

To understand the interaction mechanism between graphene oxide (GO) and typical phytopathogens, a particular investigation was conducted about the antimicrobial activity of GO against two bacterial pathogens (*P. syringae* and *X. campestris pv. undulosa*) and two fungal pathogens (*F. graminearum* and *F. oxysporum*). The results showed that GO had a powerful effect on the reproduction of all four pathogens (killed nearly 90% of the bacteria and repressed 80% macroconidia germination along with partial cell swelling and lysis at 500 μg mL^{-1}). A mutual mechanism is proposed in this work that GO intertwinds the bacteria and fungal spores with a wide range of aggregated graphene oxide sheets, resulting in the local perturbation of their cell membrane and inducing the decrease of the bacterial membrane potential and the leakage of electrolytes of fungal spores. It is likely that GO interacts with the pathogens by mechanically wrapping and locally damaging the cell membrane and finally causing cell lysis, which may be one of the major toxicity actions of GO against phytopathogens. The antibacterial mode proposed in this study suggests that the GO may possess antibacterial activity against more multi-resistant bacterial and fungal phytopathogens, and provides useful information about the application of GO in resisting crop diseases.

Received 16th September 2013
Accepted 13th November 2013

DOI: 10.1039/c3nr04941h

www.rsc.org/nanoscale

1. Introduction

Since graphene (GN) was first isolated in 2004,[1] as a single-atom thick, two-dimensional sheet of hexagonally arranged carbon with interesting physical properties, it has sparked great excitement in large-scale fields, with applications ranging from optoelectronics,[2] high-energy physics,[3] to material science[4] and biomedicine.[5] In the last few years, it was reported that graphene oxide (GO) nanowalls exhibited strong antibacterial activity towards both food-borne Gram-positive and Gram-negative bacteria.[6] Also, as reviewed by Liu *et al.*,[7] the comparison of the antibacterial activities of four graphene-based materials (graphite (Gt), graphite oxide (GtO), GO, and reduced graphene oxide (rGO)) toward *Escherichia coli* (*E. coli*) found that GO dispersion showed the highest antibacterial activity, with 89.7% of loss viability at 40 μg mL^{-1}. Recently, an exceptional application of graphene in controlling plant pathogens in biological science has been put forward. Two encouraging studies have demonstrated that GO displayed superior inactivation effects on copper-resistant *Ralstonia solanacearum* (*R. solanacearum*) and *Xanthomonas oryzae pv oryzae* (*Xoo*).[8,9] However, most prior studies are focused on the antibacterial effect of GO on bacteria, and relative few reports are available about its antibacterial effect on fungal pathogens. Montree Sawangphruk reported that rGO, which is similar to GO in property, could inhibit the mycelial growth of three fungi, *i.e.*, *Aspergillus niger*, *Aspergillus oryzae*, and *Fusarium oxysporum*,[10] which belong to unicellular eukaryote, one important member in the microbial family. Still, the toxicity action of GO against phytopathogens is not yet very well understood.

The antibacterial activity of graphene, in particular GO, is associated with its unique optical and electrical, mechanical and thermal properties,[11] such as facile surface modification, high mechanical strength, good water dispersibility, and photoluminescence.[11] Owing to these excellent antibacterial properties, GO has been exploited for biomedical and environmental management applications and successfully employed on food package,[12] medical disinfection[13,14] and water disfection.[15] Furthermore, the interesting promotional bactericidal performance of GO may open a new avenue for its application in controlling crop diseases. The crop diseases infected by a vast array of phytopathogenic fungi and bacteria can cause a 20–40% yield loss in susceptible cultivars over the world.[16,17] Long-term and extensive exposure of microorganisms to various bactericides and antibiotics has developed strong resistance which is

State Key Laboratory of Agricultural Microbiology, College of Science, Huazhong Agricultural University, Wuhan, 430070, P.R. China. E-mail: hyhan@mail.hzau.edu.cn; Fax: +86-27-87288246; Tel: +86-27-87288246

† Electronic supplementary information (ESI) available. See DOI: 10.1039/c3nr04941h

insurmountable and extremely widespread, impelling the production of multidrug-resistant pathogens.[18,19] Especially, fungal pathogens can generate asexual conidia or sexually derived ascospores to initiate the infection cycle. The specialized reproductive structures can survive for extended periods even with little or no nutrients.[20] Therefore, developing superior alternatives is essential. Given the fact that GO elicited adverse responses from prokaryotic or bacterial cells as well as eukaryotic mammalian cells.[6,7,21] One question about the application of GO as an antimicrobial agent is whether the graphene oxide with antibacterial properties can resist the infectious bacterial pathogens and fungal spores, or whether it possesses an broad-spectrum antimicrobial activity against plant pathogens.

Commonly, the widely recognized mechanisms of the antibacterial activity of graphene oxide include the synergistic effects of membrane disruption of the cell envelope and oxidative stress, which are related with the physical and chemical properties of GO.[6,7] However, to the best of our knowledge, the information about the toxicity mechanism of GO against plant phytopathogen is still very limited, especially the antifungal action mode of graphene oxide remains in the infancy stage. Without exception, the four pathogens tested in this study have been susceptible to various bactericides, and have become multidrug-resistant and more potent pathogens, and particularly the spores, one of the hardiest forms of fungus life known, can also survive severe environmental stresses such as high temperature, strong acid and high pressure. Due to the increase of the bacterial and fungal resistance to the classical agricultural chemicals, more knowledge of the action mechanism of GO towards phytopathogens is required for its potential use as an effective alternative control of phytopathogens.

The objectives of the current study were to investigate for the first time the anti-phytopathgenic activity of GO towards four typical wheat phytopathogens *in vitro* and explored the interaction mechanism of GO with them. The phytopathogens used included two bacterial pathogens (*Pseudomonas syringae* (*P. syringae*), *Xanthomonas campestris pv. undulosa* (*X. campestris pv. undulosa*)) and two fungal pathogens (*Fusarium graminearum* (*F. graminearum*) and *Fusarium oxysporum* (*F. oxysporum*)), all of which can cause infection to many Triticum genera and induce catastrophic diseases such as Fusarium head blight (FHB), bacterial leaf streak (BLS) and bacterial leaf blight (BLB).[22–25] The Gram-negative bacterium *P. syringae* is even pathogenic to more than 50 different crop plants. Our findings indicate that GO with a broad-spectrum and high-efficiency antimicrobial activity against multidrug-resistant pathogens may have the potential as an alternative or complement to chemical pesticides for the control of phytopathogens.

2. Experimental sections

2.1. Preparation of graphene oxide

GO was prepared from natural graphite powders by the modified Hummers method.[26] Briefly, the natural graphite powders (99.99%; Sigma-Aldrich) were initially oxidized by concentrated sulfuric acid (H_2SO_4) to produce graphite oxide (GtO). After being filtered and washed with deionized water to remove chemical residues, the produced GtO dispersed in deionized water was bath-sonicated (Elamsonic, S60H) for 3 h to exfoliate and obtained the GO mixture.

2.2. Instrumentation

Several instruments were used to characterize and analyze the physical and chemical properties of GO samples, including atomic force microscope (AFM), transmission electron microscope (TEM), Raman spectrometer, and Fourier-infrared spectrometer (FT-IR spectrum). A drop of dispersion was spread on a freshly cut mica surface and the samples were air-dried for AFM analysis (Agilent 5500). The morphology of graphene was characterized by TEM (Hitachi H-7650, Japan). The Raman spectra were obtained in Via Raman spectrometer (Renishaw, UK) equipped with a confocal microscope (Leica, DM LM/P/11888500, Germany). FT-IR spectra were recorded on a Nicolet Avatar-330 spectrometer with 2 cm^{-1} resolution using the KBr pellet technique.

2.3. Strains and phytopathogens culture

In this experiment, four representative phytopathogens with parasitism on crop were selected, including two bacterial pathogens (*P. syringae* and *X. campestris pv. undulosa*) and two fungal pathogens (*F. graminearum* and *F. oxysporum*). The four microbes were all purchased from the State Key Laboratory of Agricultural Microbiology of Huazhong Agricultural University (Wuhan, China).

P. syringae and *X. campestris pv. undulosa* were grown in LB (Luria–Bertani) broth medium in a humidified incubator at 30 °C with constant agitation overnight. The bacterial cultures were harvested in the midexponential growth phase and the cells were collected by centrifugation at 6000 rpm for 5 min. Subsequently, the bacteria bread was washed three times with deionized water to wipe off the medium constituents and other chemical macromolecules. Finally, the cells were re-suspended in deionized water (DI) and the suspensions were progressively diluted to a desired concentration of 10^7 to 10^8 colony forming units (CFU per mL).

F. graminearum and *F. oxysporum*, two filamentous pathogenic fungi, were grown on potato dextrose agar (PDA) slant at 28 °C. After five days of incubation in an incubator, *F. graminearum* spores were obtained as described previously.[27] The mycelia of *F. oxysporum* were incubated in 3% green bean soup liquid medium and maintained for 5 days under light conditions with gentle shaking to obtain macroconidia suspensions. Differently, the spores of *F. oxysporum* fungus were obtained by washing their mycelia with DI water. After filtering the resulting macroconidia suspensions through sterilized gauze, the conidia were harvested by centrifugation at 3500 rpm for 5 min and washed twice with sterile distilled water. The spore suspensions were first adjusted to a desired concentration of 3×10^7 spores per mL. All experiments were carried out at room temperature.

2.4. *In vitro* antimicrobial assays

Studies of bacterial cell growth and viability. Bacterial growth was assayed as reported in our previous work.[8] 200 μL of

the diluted cell suspensions (10^7 to 10^8 CFU per mL) was mixed with 20 μL of five different concentrations of GO (10, 50, 100, 250, and 500 μg mL^{-1}) and incubated at 30 °C for 2 h with gentle shaking. A control sample contained 200 μL of the cell suspensions and 20 μL of deionized water. The mixture was then transferred to 5 mL tubes, each containing 2 mL LB medium, and the tubes were inoculated on a rotary shaker at 120 rpm and 30 °C. The value of optical density (OD) at a wavelength of 600 nm was measured on a Nicolet Evolution 300 UV-VIS spectrometer every hour. Bacterial growth curves were created by plotting OD values *versus* time. All treatments were prepared in triplicate.

For antibacterial activity test, the bacteria (10^7 to 10^8 CFU per mL) were incubated with different concentrations of GO for 2 h, and then 20 μL of a serial 10^6-fold dilution of each bacterial suspension in sterile deionized water was spread onto LB plates and left to grow for two days at 30 °C. Colonies were counted and the cell mortality (% of the control) was expressed as the percentage of (counts of the control – counts of the treated samples)/counts of the control. All treatments were individually repeated at least three times.

Studies of spore germination. *F. graminearum* spores were prepared as described previously.[27] 100 μL of spore suspensions (3 10^7 spores per mL) were mixed with 100 μL of GO in the tubes to obtain a final concentration of 10, 50, 100, 250 and 500 μg mL^{-1}. Control samples contained spore suspensions and 20 μL of deionized water. Then, 50 μL mixture with a different concentration of GO was transferred onto sterile concave slides for incubation at 28 °C for 7 h (for *F. graminearum*) and 5 h (for *F. oxysporum*) in complete darkness. The humidity level was maintained at 100% during germination. Three concave slides were prepared for each treatment and the mean values were compared. Two hundreds of spores per treatment were assessed by measuring the germination rate and the length of the germ tubes. Micrographs were taken with a digital camera connected to a Leica microscope (Germany DCF425). The spore germination rate was calculated as follows:

$$\text{Spore germination rate (\%)} = (\text{the number of germinated spores})/(\text{total number of spores}).$$

2.5. Fluorescence microscopy imaging

Briefly, a 1 mL portion of bacterial suspensions (10^7 to 10^8 CFU per mL) and 100 μL of GO (500 μg mL^{-1}) were mixed in the centrifuge tube, and then the mixture was incubated at 30 °C for 2 h with gentle shaking. After being harvested by centrifugation in a microcentrifuge at 6000 rpm and suspended in 1 mL of water, the cells were stained with 10 μL propidium iodide (PI; excitation/emission at 535 nm/617 nm; Sigma-Aldrich) for 15 min and then counter-stained with 10 μL 4′-6-diamidino-2-phenylindole (DAPI, excitation/emission at 358 nm/461 nm; Sigma-Aldrich) for 5 min in the dark.[28] For fungi, 80 μL of fresh conidial suspensions (3×10^7) was treated with 80 μL of GO (500 μg mL^{-1}) at 28 °C for 3 h and then the mixture was stained by the fluorescent dye as described above. Control cell samples were treated with deionized water. Subsequently, the test samples were observed under an inverted fluorescence microscope (Eclipse Ti, Nikon). The cell death percentage was the ratio of the number of cells stained with PI (dead bacteria) to the number of cells stained with DAPI plus PI (total bacteria).

2.6. Cell morphology observation with SEM

The morphological changes of bacterial cells and spores were further investigated using SEM after treatment with GO. The bacterial suspensions were treated with GO for 2 h at 30 °C and the spore suspensions were treated with GO for 3 h at 28 °C. After centrifugation at 6000 rpm for the bacterial cells and 3500 rpm for the conidia, the condensed cells were fixed with 2.5% glutaraldehyde, postfixed with 1% aqueous OsO4 (Fluka) and washed with 0.1 M, pH 7.0 phosphate buffers. Subsequently, the samples were dehydrated in an ascending ethanol series (30, 50, 70, 80, 90 and 100%) for 15 min, respectively and dried in a vacuum oven. Finally thin sections containing the cells were placed on the copper grids and observed under a SEM (JEOL JSM-6700F).[7]

2.7. Measurement of bacterial membrane potential

The measurement of membrane potential has been used as an indicator of viability in numerous studies to test the susceptibility to antimicrobial agents.[29,30] The bacterial membrane potential after treatment with GO was measured using the BacLight Bacterial Membrane Potential Kit (Molecular Probes, Invitrogen). The kit contained a fluorescence dye $DiOC_2$ (3,3′-diethyloxacarbocyanine iodide), which exhibits green fluorescence in all bacterial cells, but the fluorescence shifts toward red emission as the dye molecules self-associate at the higher cytosolic concentrations caused by larger membrane potentials. When the pathogens were exposed to the proton ionophores CCCP (carbonyl cyanide 3-chlorophenylhydrazone), CCCP could destroy the membrane potential by eliminating the proton gradient, and thus was used as a positive control in this study. The experiment was performed as described in the kit manual. Briefly, bacteria obtained from log-phase cultures were diluted to approximately 1.0×10^6 cells per mL in filtered PBS. Subsequently, 1 mL of the bacterial suspension was supplemented with 10 μL of 3 mM $DiOC_2$ (3). Meanwhile, 10 μL of 500 μM CCCP was added into the depolarized control sample and 10 μL of water, into the unstained control sample. After incubation at room temperature for 15–30 minutes, all the samples were assayed with a flow cytometer (FACSCalibur, USA) equipped with a laser emitting at 488 nm. Fluorescence is collected in the green and red channels ("GC" and "RC"). 1.0×10^4 cells were collected for every sample.

2.8. Measurement of electrolyte leakage

Electrolyte leakage assay was performed as described by Steel *et al.*[31] Electrical conductivity of the fungal spore suspension was measured using a conductivity meter (ES-12, Horiba, Japan). The total electrolyte loss was measured 2 h after the addition of chloroform into the fungal spore suspension at the end of each experiment.

2.9. Statistic analysis

All the experiments were performed in triplicate and the results were expressed as mean ± SD (standard deviation). Statistical analysis was implemented using Statistical Product and Service Solutions software (SPSS) (SPSS 11.0, United States). The differences between the groups were assessed using the analysis of variance test. The results were considered statistically significant when the P value was <0.05 or <0.01.

3. Results and discussion

3.1. Physical and chemical characterization of GO

In the study, GO was synthesized by oxidizing natural graphite powders using H_2SO_4 and $KMnO_4$ according to the classical modified Hummers method.[26] TEM and AFM microscopes were used to investigate the morphological structure of GO (Fig. 1). As can be seen in Fig. 1a, the AFM image of exfoliated GO suspensions at 100 μg mL^{-1} and the GO exhibited a flat-sheet structure with an average thickness of 0.794 nm. The representative TEM image in Fig. 1c revealed that the GO sheet was thin, transparent and smooth with small wrinkles. In Fig. 1b, two representative bands could be observed in the Raman spectrum of GO. The G band was broad and shifted to 1590 cm^{-1} and the D band at 1350 cm^{-1}, due to the extensive oxidation, and the ratio of D/G intensity of GO was 0.849. Meanwhile, as indicated by the FT-IR spectrum in Fig. S1 (ESI, Fig. S1†), the characteristic vibrations of GO included the broad and intense peak of –OH group at 3423 cm^{-1}, the strong C═O peak at 1750 cm^{-1}, the C–OH stretching peak at 1200 cm^{-1}, and the C–O stretching peak at 1050 cm^{-1}.

3.2. *In vitro* antibacterial activity of GO

The antibacterial activity of GO toward selected bacterial pathogens was investigated by measuring the growth curve and the cell viability after the exposure of the pathogens to GO. The bacteria (or bacteria treated with graphene oxide) were cultivated in LB medium and the value of optical density at OD600nm was monitored over different time periods (from lag phases to stationary phases) utilizing a UV-Vis spectrometer. As illustrated in Fig. 2a and b, GO can significantly inhibit the bacterial growth in the range 10 to 500 μg mL^{-1} of GO. A growth delay of 4 h and 5 h occurred for *P. syringae* and for *X. campestris pv. undulosa* respectively, when incubated with 500 μg mL^{-1} of GO, respectively, in the onset of the logarithmic growth phase, referred to as bacteriostatic condition. Fig. 2c shows the corresponding cell viability of the two bacterial pathogens after treatment with various concentrations of GO (10–500 μg mL^{-1}), with the survival rate being 95.00%, 85.91%, 48.22%, 26.34%, 15.13% and 11.20% for *P. syringae* and 93.04%, 81.94%, 63.12%, 36.34%, 19.13% and 13.20% for *X. campestris pv. undulosa*. The results indicated that the bacterial cell loss gradually soared with the increasing concentration of GO, which was confirmed by the consecutively decreasing number of colonies grown on the LB plates, referred to as bactericidal effect (ESI, Fig. S2†). However, a tiny minority of cells were observed at the highest concentration of GO, suggesting that very few *P. syringae* and *X. campestris pv. undulosa* pathogens retain their viability, or rather, GO induces nearly 90% cell death at a high concentration. Therefore, it can be concluded from the above results that GO exhibits strong antibacterial activity against plant bacterial pathogens.

3.3. *In vitro* antifungal activity of GO

The germination of dormant spores is the first crucial step in the return of spores to vegetative growth.[32] In this study, the conidia of both *F. graminearum* and *F. oxysporum* were germinated on the concave slide in the presence of 10–500 μg mL^{-1} of GO at 28 °C.[27] The results showed that GO displayed dose-dependent inhibitory effects on both *F. graminearum* and *F. oxysporum* spore germination and germ-tube elongation (Fig. 3). When the spore germination rate reached 97.65% in the control, the *F. graminearum* spore germination rate was 78.34%, 63.28%, 58.09%, 38.98% and 14.51%, respectively, after treatment with five different concentrations of GO (Fig. 3a), and *F. oxysporum* showed a similar trend in spore germination rate, *i.e.*, 82.69%, 74.89%, 47.27%, 27.18% and 18.84% (Fig. 3b) compared with 96.39% of the control samples. Meanwhile, GO was also observed to have a significant effect on sporoduct growth and germination pattern. The conidia germinated in control conditions developed germ tubes with a length of 35.19 μm for *F. graminearum* and 44.5 μm for *F. oxysporum*, whereas the germ tubes of the GO-treated spores were concentration-dependently inhibited. The germ tube length was only 9.78 μm for *F. graminearum* and 6.1 μm for *F. oxysporum* when treated with the highest dose of GO (500 μg mL^{-1}), which was a 71.95% and 82.26% decrease in length against the control (Fig. 3c). Normally, *Fusarium* conidia displayed a bipolar germination pattern in which germ tubes mostly developed from apical cells.[33] When exposed to GO at an increasing dose, a larger proportion of interstitial germ tubes occurred (Fig. 3d). As shown in Fig. 4c, long and normal germ tubes could be observed visually in the control samples. However, most germ tubes of the spores immersed in the highest concentration of GO (500 μg mL^{-1}) developed from the side of spores (red arrows) and their apical cells were swollen and then stopped growing (blue arrows), and some even still remained in the original form without any germ tubes (Fig. 4d). Fig. S3† shows the corresponding photomicrograph of spore germination after treatment with various concentrations of GO, which has visually confirmed that GO can effectively restrain the spore germination of both pathogens. Even 12 h after incubation at 500 μg mL^{-1} and 1000 μg mL^{-1}, most of the spores were still inhibited in germination (Fig. S4 in the ESI†). It can be deduced from these observations that GO treatment can remarkably reduce macroconidia viability. The spore maturation and germination are essential developmental steps in the fungal life cycle and critical for plant colonization.[32] In favourable growth conditions, the spore germinates and goes through outgrowth, ultimately being converted back into a growing mycelium, but once the germination of spore is inhibited or stopped, the spore can not develop into mature mycelium and initiate the infection cycle.

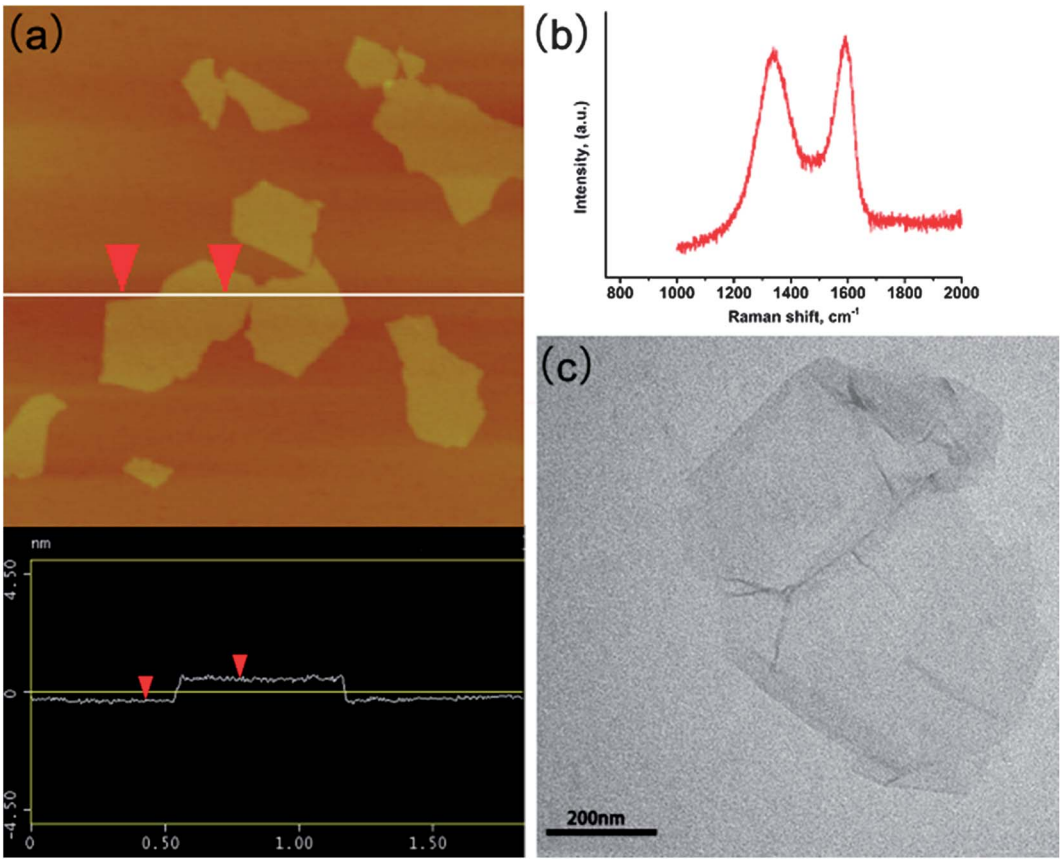

Fig. 1 Characterization of synthesized GO. (a) AFM images of graphene oxide (GO) sheets and the corresponding height profiles; (b) Raman spectra of GO; and (c) TEM images of GO sheets.

3.4. Fluorescence microscopy observations

The antimicrobial activity of GO against phytopathogens was further verified using fluorescent dyes of propidium iodide (PI) and 4′-6-diamidino-2-phenylindole (DAPI). The DAPI dye can pass through live cells with intact membrane and bind strongly to DNA, which emits blue fluorescence, while the PI dye is membrane-impermeable and commonly used to stain cells with damaged or compromised membranes and emits red fluorescence, which is usually indicative of dead cell.[28] As shown in Fig. 5, the average percentages of viability loss (*i.e.*, PI-stained) for bacterial cells and conidial cells are significantly increased compared to that of the control. Additionally, the bacteria *X. campestris pv. undulosa* in Fig. 5a and *P. syringae* in Fig. 5c were almost vigorous in the control condition (Fig. 5a and c), while exposed to 500 μg mL^{-1} GO, both pathogens were significantly killed and some of them aggregated together, as shown in Fig. 5b and d.

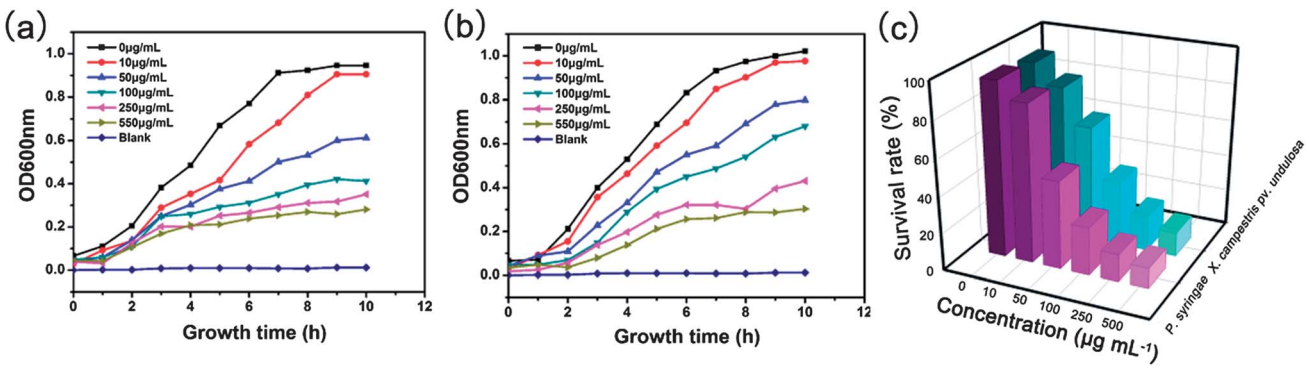

Fig. 2 Growth curve of *P. syringae* (a) and *X. campestris pv. undulosa* (b) after incubation with and without different concentrations of GO. (c) Bacteria cell viability measurements after incubation with different concentrations of GO.

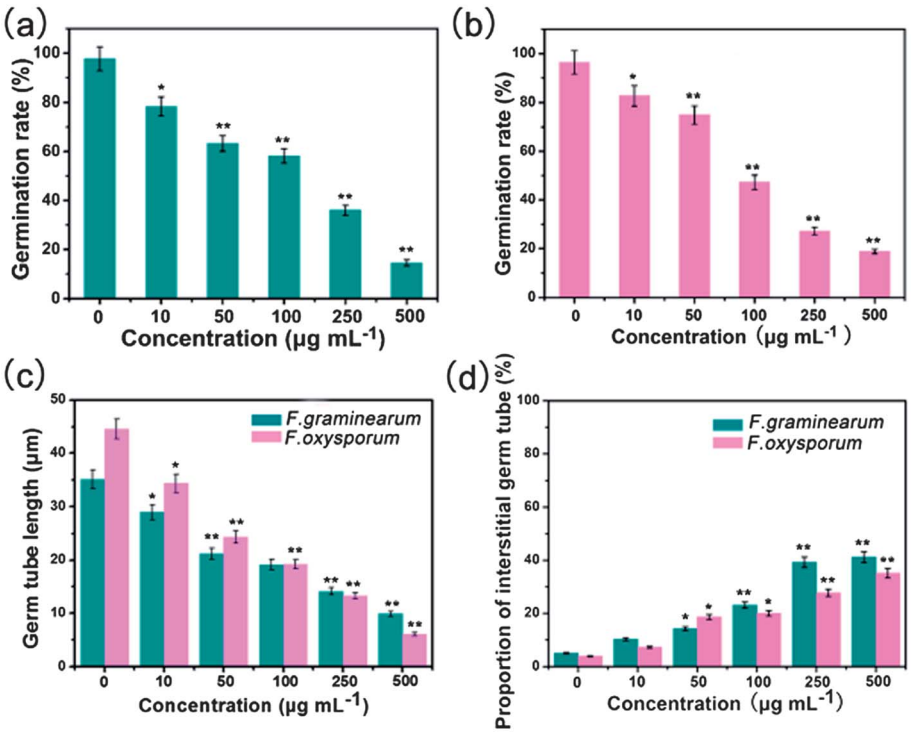

Fig. 3 (a) The germination rate of *F. graminearum* and (b) *F. oxysporum* conidia after incubation with different concentrations of GO sheets. *F. graminearum* or *F. oxysporum* conidia (3×10^7) were blended with an identical volume of GO solution and 50 μL mixture was germinated on concave slides for 7 h or 5 h at 28 °C, respectively. (c) The germ tube length and the proportion of interstitial germ tubes of both conidia after incubation with different concentrations of GO sheets. Error bars represent the standard deviation.

3.5. Intertwinding the phytopathogens by GO sheets and cell lysis

The above results imply that the direct incubation of phytopathogens with GO sheets is essential for the inactivation of bacterial pathogens and cells. Thus, to explore the interaction between GO and pathogens *in vitro* and the antibacterial mechanisms, the results from the fluorescence-based assay were further substantiated with SEM imaging at a 500 μg mL^{-1} dose of GO. Ultrastructural examination found that the bacterial cells and fungal spores treated with water possessed a natural, intact and relatively smooth cell wall or plasma membrane envelope and an unbroken cytoarchitecture (Fig. 6a, c, e and g).[27] However, as illustrated in Fig. 6, after exposure to 500 μg mL^{-1} GO, *P. syringae* and *X. campestris pv. undulosa* were wrapped up or stabbed by GO sheets and the cells became deformed and collapsed (Fig. 6f and h); even the whole spore of *F. graminearum* and *F. oxysporum* with a length of several micrometers was intertwined by the thin sheets of GO (Fig. 6b1 and d1).

3.6. Perturbation of membrane integrity by GO

Decrease of membrane potential. The direct contact of pathogens with GO showed that the pathogens were wrapped by the GO sheets, suggesting that GO may have the potential to perturb the plasma membrane integrity of pathogens. To test this hypothesis, we examined whether the bacterial membrane potential changed. Membrane potential (MP) plays a critical role in bacterial metabolism processes, not only in the generation of ATP,[34] but also in chemotaxis,[35] glucose transport[36] and so on. Changes in the membrane potential can be visualized by the ratio of red to green fluorescence intensity measured by flow cytometry. In the study, CCCP can destroy membrane potential by eliminating the protongradient and was used as the positive control. As demonstrated in Fig. 7a, both pathogens showed a significant difference in red/green ratio after treatment with GO at a concentration of 50 μg mL^{-1} or higher. An increased concentration caused a higher rate of reduction, which confirmed that GO could indeed damage the membrane integrity of pathogens.

Loss of electrolytes. The disrupted cell membrane of the fungal spores was verified by examining the leakage of electrolytes from *F. graminearum* and *F. oxysporum* cells exposed to GO. The results indicated that about 57.7% of the total electrolytes leaked out of the *F. graminearum* cells and 53.6% out of *F. oxysporum* even 300 min after exposure to 500 μg mL^{-1} GO, suggesting that GO could indeed disrupt the phospholipids of fungal membranes (Fig. 7b). Injury was manifested as an increased leakage of electrolyte. The disruption of membrane has a large impact on the membrane potential changes and membrane-associated energy-transducing system, such as intra- and extra-cellular ATP pools.[37] One previous study has proved that the activation of membrane potential is associated with spore germination. One of the earliest events in the germination of *Fusarium* spores is the activation of membrane potential.[33] Thus, the perturbation of membrane integrity and the subsequent leakage of electrolytes may have relationship with inactivation of spores caused by GO.

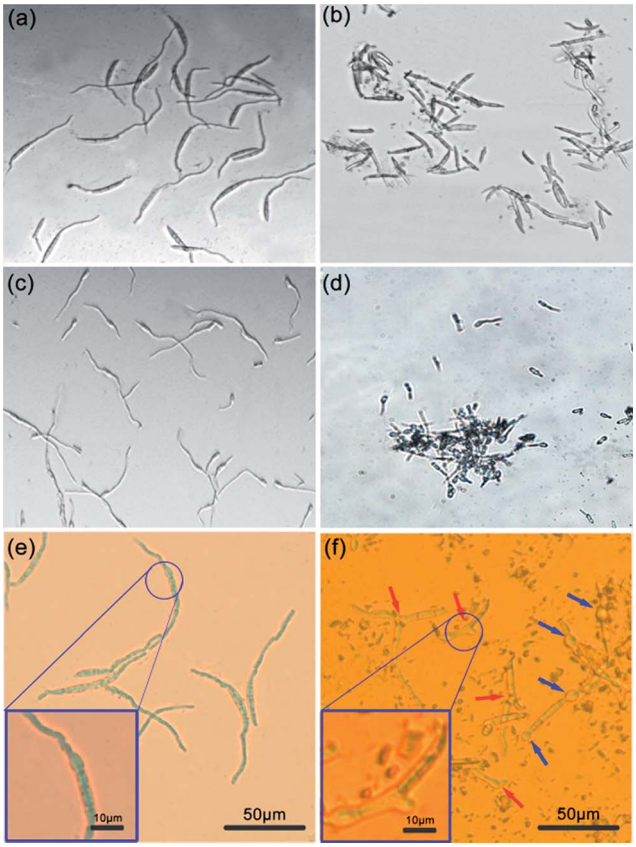

Fig. 4 Photomicrograph of GO-induced macroconidia germination. *F. graminearum* conidiu were germinated on coverslips for 7 h at 28 °C (a) without (the control) and (b) with 500 μg mL^{-1} of GO. *F. oxysporum* conidia were germinated on concave slide for 5 h at 28 °C (c) in the control condition and (d) 500 μg mL^{-1} of GO. (e) The germination pattern of *F. graminearum* spores under water. (f) The germination pattern of *F. graminearum* spores under 500 μg mL^{-1} of GO. Insets in (e) and (f) are the partial magnification.

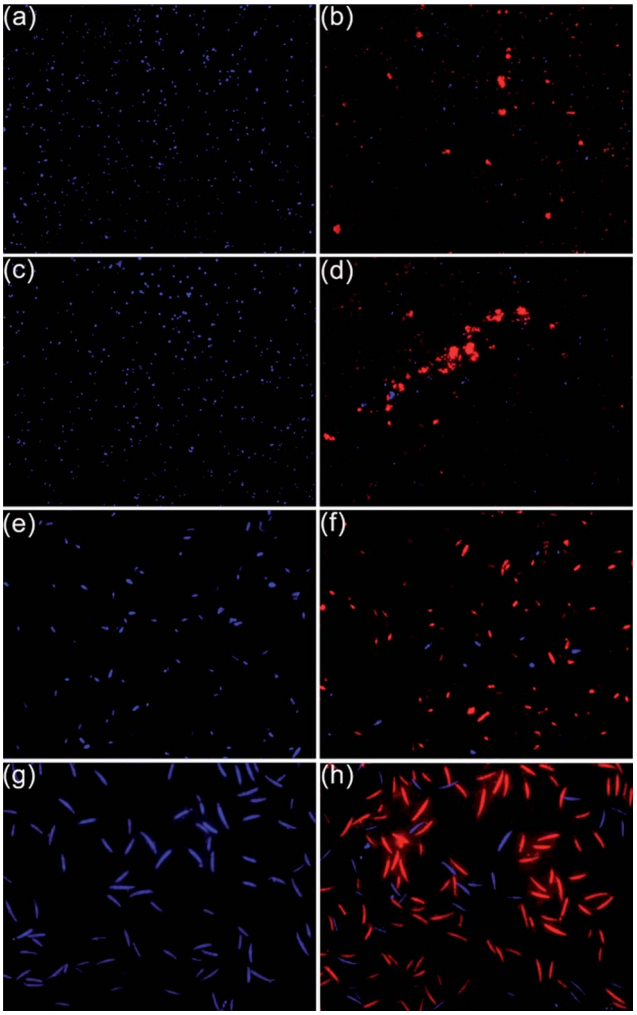

Fig. 5 Cell viability measurements by fluorescence microscopy. Fluorescence microscope images of (a) *X. campestris pv. undulosa*, (c) *P. syringae*, (e) *F. oxysporum*, and (g) *F. graminearum* after being stained with propidium iodide (PI) and DAPI without GO dispersions. (b, d, f and h) Fluorescence microscope images of total cells (cells stained with PI and DAPI) after exposure to GO (500 μg mL^{-1}). Fluorescence assay shows the antimicrobial activity of GO as the percentage of bacteria or spores stained with PI (red colour) or the percentage of loss of viability.

The above results indicate that the GO can display broad-spectrum antimicrobial activity towards bacterial and fungal phytopathogens and the antimicrobial activity is dose-dependent. Interestingly, further analysis of the interaction between GO and the four types of pathogens, including bacterial pathogens and fungal spores, found that they were all trapped or wrapped by the thin sheets of GO and subsequently formed agglomerates as shown in the SEM images in Fig. 6. It is worth noting that in this work, the only difference between the treated samples and the control in the mixture is the GO thin sheets. Previous observations have shown that carbon CNTs can wrap around human gut bacteria and diameter-dependently pierce the cell wall and membranes.[38] Embedded CNTs can also influence the conformation of individual lipid molecules, the organization of membrane molecules, and the diffusion behavior of lipidmolecules of biomembrane.[39] In terms of molecular structure, the large two-dimensional graphene sheets are formed by longitudinal unzipping of carbon nanotubes with extremely similar properties to nanotubes.[11] Recently, O. Akhavan *et al.* also reported that the graphene (oxide) suspensions wrapped the *E. coli* bacteria within the aggregated sheets and the cells were biologically disconnected from their environment, thus being unable to proliferate and photothermally inactivated forever by near-infrared irradiation.[15]

Recent publications of charged nanoparticles on electroneutral phospholipids bilayers revealed that electrostatic attraction improved the adhesion of a charged nanoparticle to the membrane, where the increase of electrostatic energy results in almost full wrapping of the charged nanoparticle by the membrane.[40] What is more, graphene or GO has been proved theoretically to absorb amino acid and other biological molecules such as nucleic acids and peptides, onto their sheets,[41,42] and this unique capacity creates a robust platform for intracellular biotherapy.[43] Moreover, the binding strength of GO to those molecules is found to be stronger than that of CNTs.[44] Therefore, as observed in our results, similar effects may occur between these pathogens and graphene oxide. In our

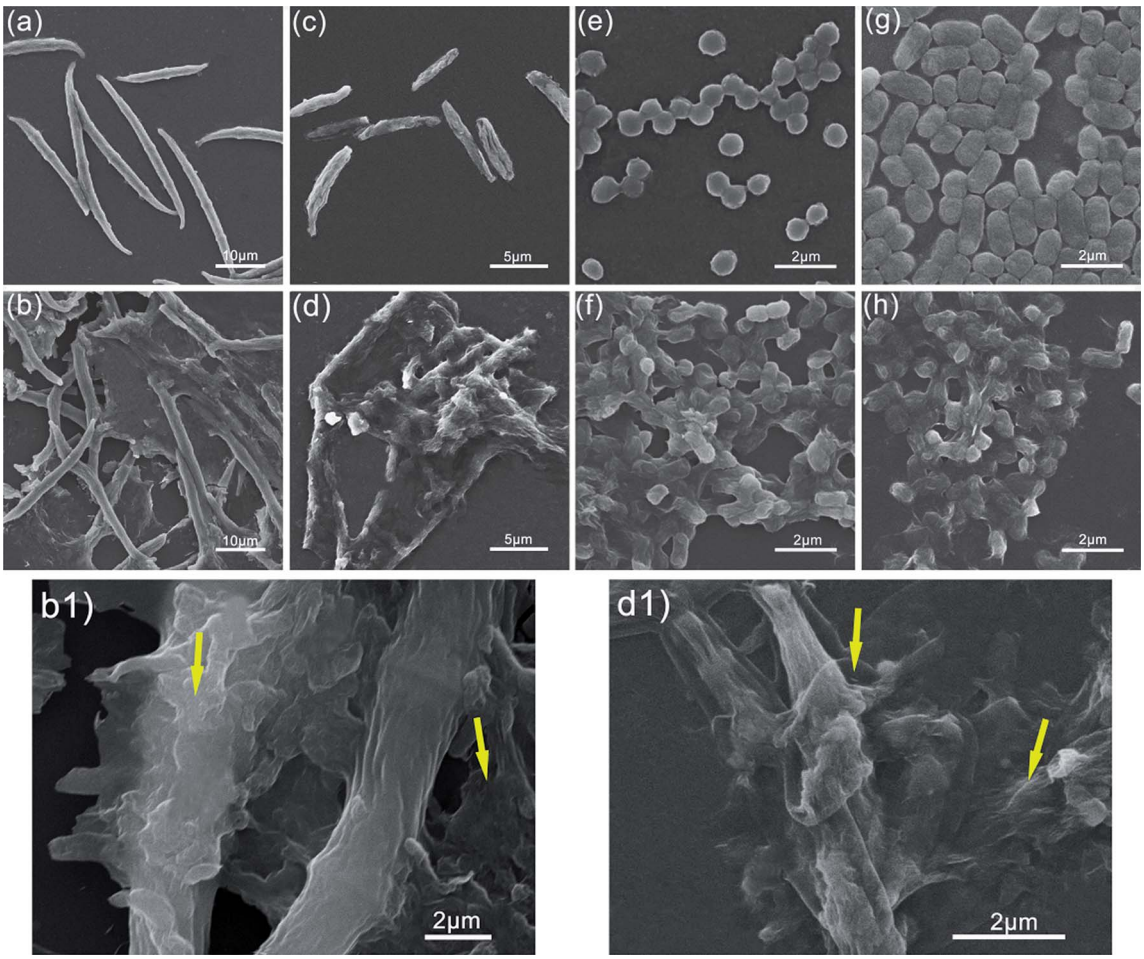

Fig. 6 SEM images of (a) conidia of *F. graminearum* and (c) *F. oxysporum* after incubation with sterile water for 3 h without GO sheets; (b) conidia of *F. graminearum* and (d) *F. oxysporum* after incubation with GO (500 μg mL^{-1}) for 3 h; (e) *P. syringae* without GO; (f) *P. syringae* with GO (500 μg mL^{-1}) for 2 h; (g) *X. campestris pv. undulosa* without GO; and (h) *X. campestris pv. undulosa* with GO. (b1) and (d1) are *F. graminearum* and *F. oxysporum* spores exposed to 500 μg mL^{-1} GO, respectively, at 8000× magnification.

experiments, the cell wall of Gram-negative bacterial pathogens has a peptidoglycan laye (also called mucopetide) of about 7–8 nm.[45] Once in contact with bacteria and spores, GO sheets interwind the pathogens and the membrances are most likely blocked by the GO covering, implying that the GO sheets could interfere with the absorption of nutrient or block water channels of biological cells,[46] and also disturb normal metabolism of microbes, just like GO blocks the substance exchange of A549 cells.[47] Especially for conidia, the surface region of spore membrane contains the receptors for germinants as well as the enzymes that are involved in the depolymerization of the spore cortex.[48] And analysis of the above results demonstrated that the inactivation process of pathogens may be found to be the synergy of multiple toxicity action. When the conidia are twined with GO sheets to form spore-GO congeries and affect the substance exchange of spore wall or membrane, the germination process of spore is inhibited, inducing abnormal morphology or growth obstruction of germ tubes, followed by cell swelling and lysis.

Another possible mechanism proposed for GO nanosheet-mediated membrane rupture process is directly illustrated in the membrance integrity assays. Previous studies have put forward that for the membrane damage mechanism of SWCNT, by which, SWCNT, another needle-like structure carbon nanomaterial with physicochemical characteristics similar to GO, may easily penetrate through the outer membrane and the thin peptidoglycan layer in the bacteria.[39] Another systematic analysis by Mickaël Lelimousin *et al.* has demonstrated the mechanism of spontaneous exothermic insertion of CNTs into cell lipid bilayer membranes by molecular simulations.[38] In the current study, the second assay indicated that the bacterial membrane potential was reduced and the electrolyte of fungal spores leaked when exposed to GO dispersions. Usually, a lowered membrane potential or leakage of electrolyte is accompanied by membrane damage.[37] The results showed that the pathogens may suffer from perturbation of membrane integrity, though the injury was not obviously observed in the SEM images. Further, the membrance integrity assays and the SEM results could enable us to speculate on a local perturbation of membrance induced by GO sheets and the wrapping mechanism has great relationship with the membrance changes. It could hardly be assumed to be that GO treatment can maintain

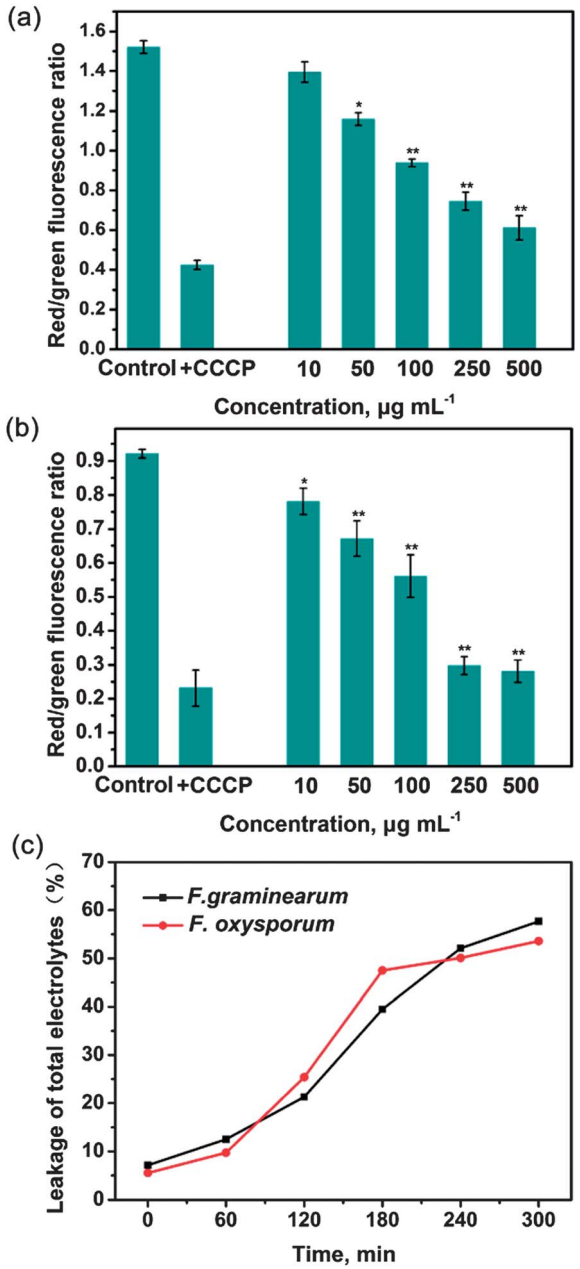

Fig. 7 Measurement of cell membrane potential in (a) *X. campestris pv. undulosa*, (b) *P. syringae* after exposure to different concentrations of GO and the loss of electrolytes in (c) *F. graminearum* and *F. oxysporum* after exposure to different concentrations of GO. Fluorescence ratio indicates the membrane potential. The fluorescence ratio is the mean of red to green fluorescence intensities measured by flow cytometry. CCCP (carbonyl cyanide 3-chlorophenylhydrazone) can destroy membrane potential by eliminating the proton gradient and was used as a positive control. Statistical significance was calculated using Student's *t*-test between control and GO-treated groups. * and ** indicate $p < 0.05$ and $p < 0.01$.

the bacterial membrane integrity. It is reported that GO nanosheets can produce either disorganization of cell membrane or oxidative stress against major foodborne pathogens like *E. coli* and *S. aureus*.[6,7] This effectiveness of graphene as an antimicrobial agent can be attributed to its extraordinary properties, such as good thermal stability, high surface area, exceptional physiochemical properties, high electronic conductivity and excellent mechanical strength.[3,6,11] Alexey V. Titov *et al.* demonstrated by coarse-grained molecular dynamics (CGMD) simulations that graphene sheets could be hosted horizontally or vertically inside the phospholipid bilayer formed by 1-palmitoyl-2-oleoyl-*sn-glycero*-3-phosphocholine phospholipids (POPC).[49] They found these graphene micelles merged with the membrane and released the monolayer, which penetrated the membrane and formed hybrid sandwiched graphene-membrane superstructures. The cell wall of Gram-negative bacteria is only composed of a thin peptidoglycan layer.[50] Just like CNT–lipid assemblies,[38,39] the attachment of GO sheets to the pathogens can strongly impact the cell outer membrane by piercing or laceration (Fig. 7 and 8). The change in membrane integrity probably can perturb many essential functions, such as energy transduction, transport of materials and respiration.[34–37] Those damaged bacterial cells or the spores can not repair damaged membranes and finally perish.[51]

As indicated in Fig. 8, this direct interaction mechanism between GO and pathogens (bacterial cells or fungal spores) by wrapping the cells and direct contact with the cell wall or membrane probably causes partly serious structural damages of pathogens *via* membrane depolarization, then may impacts physiological metabolism processes and finally leads to the death or growth inhibition of bacterial cells or spores shown in Fig. 2 and 3. Excessive damage can also overwhelm the capacity of repair systems during spore dormancy and lead to the death of spore.[51] The high efficiency of GO in inhibiting bacterial reproduction and sporulation suggests its potential for developing broad-spectrum antibacterial activity against other pathogenic microorganisms. Therefore, the use of GO can be expected to produce a high level of resistance in crop plants against a variety of bacterial and fungal pathogens, and serve as a long-term effective measure to control pathogenic microbes, in contrast to some chemical fungicides.

4. Conclusions

The current research aimed to investigate the powerful antimicrobial activity of GO against both bacterial (*P. syringae* and *X. campestris pv. undulosa*) and fungal (*F. graminearum* and *F. oxysporum*.) phytopathogens. Both the colony forming counts and the conidia germination rate showed that GO concentration-dependently caused mass loss of bacterial pathogens and spore germination inhibition or deformed germination. Furthermore, the subsequent analyses using fluorescent staining, SEM revealed that the bacterial pathogens and fungal spores were intertwined with GO thin sheets, forming an aggregate and locally damaging the cell membrane integrity, which probably responsible for the toxicity mechanism against both the bacterial and the fungal pathogens. Understanding the toxicity mechanisms of graphene oxide on bacteria and fungal spores is extraordinarily useful for developing new strategies to control pathogenic fungi.

The phytopathogens tested and even other more pathogenic microorganisms are also drug-resistant and are not susceptible to the conventional antimicrobial agents such as triazoles.

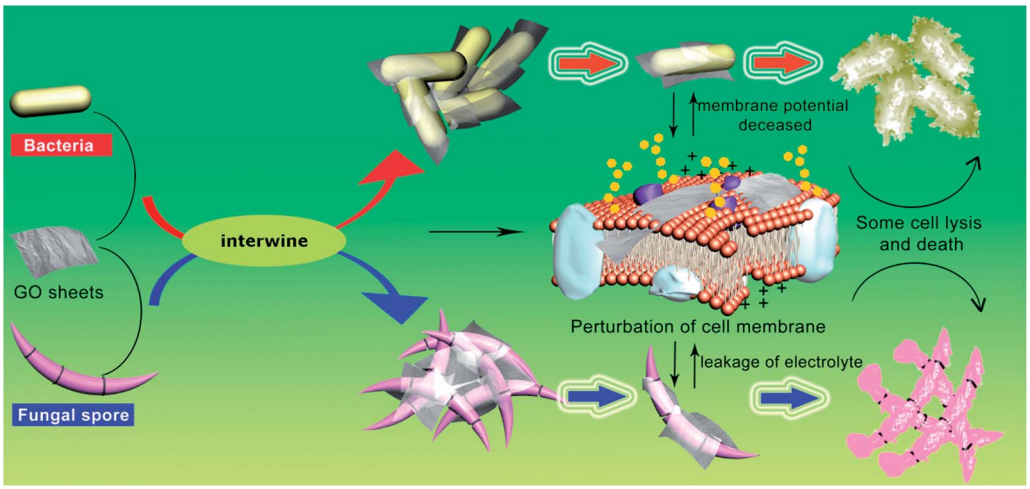

Fig. 8 Schema of interaction between GO and pathogens and the toxicity mechanisms of antibacterial activity of GO against bacterial phytopathogens and fungal spores. In this experiment, the bacterial cells and fungal spores were intertwined with a wide range of aggregated graphene oxide sheets and resulted in local perturbation of the cell membrane, which induced loss of bacterial membrane potential and leakage of electrolytes of fungal spores, and caused the lysis and death of pathogens.

Given that the antibacterial and antifungal activity of GO nanosheets stems from the physical injury to the bacterial or spore membrane, which is induced by direct interaction with pathogens, a similar complex mechanism can be applied to other phytopathogens, indicating that graphene oxide may have the potential as an antimicrobial agent to control pathogenic bacteria in crops.

Acknowledgements

The authors gratefully acknowledge the financial support for this research from National Natural Science Foundation of China (20975042, 21175051), the Fundamental Research Funds for the Central Universities (2010PY009, 2010PY139) and the Natural Science Foundation of Hubei Province Innovation Team (2011CDA115).

Notes and references

1 K. Novoselov, A. Geim, S. Morozov, D. Jiang, Y. Zhang, S. Dubonos, I. Grigorieva and A. Firsov, *Science*, 2004, **306**, 666–669.
2 F. Xia, T. Mueller, R. Golizadeh-Mojarad, M. Freitag, Y.-m. Lin, J. Tsang, V. Perebeinos and P. Avouris, *Nano Lett.*, 2009, **9**, 1039–1044.
3 K. Novoselov, A. K. Geim, S. Morozov, D. Jiang, M. K. I. Grigorieva, S. Dubonos and A. Firsov, *Nature*, 2005, **438**, 197–200.
4 C. Stampfer, E. Schurtenberger, F. Molitor, J. Guttinger, T. Ihn and K. Ensslin, *Nano Lett.*, 2008, **8**, 2378–2383.
5 H. Pandey, V. Parashar, R. Parashar, R. Prakash, P. W. Ramteke and A. C. Pandey, *Nanoscale*, 2011, **3**, 4104.
6 O. Akhavan and E. Ghaderi, *ACS Nano*, 2010, **4**, 5731–5736.
7 S. Liu, T. H. Zeng, M. Hofmann, E. Burcombe, J. Wei, R. Jiang, J. Kong and Y. Chen, *ACS Nano*, 2011, **5**, 6971–6980.
8 X. P. Wang, X. Q. Liu and H. Y. Han, *Colloids Surf., B*, 2013, **103**, 136–142.
9 J. N. Chen, X. P. Wang and H. Y. Han, *J. Nanopart. Res.*, 2013, **15**, 1–14.
10 M. Sawangphruk, P. Srimuk, P. Chiochan, T. Sangsri and P. Siwayaprahm, *Carbon*, 2012, **50**, 5156–5161.
11 V. Singh, D. Joung, L. Zhai, S. Das, S. I. Khondaker and S. Seal, *Prog. Mater. Sci.*, 2011, **56**, 1178–1271.
12 A. Arora and G. Padua, *J. Food Sci.*, 2010, **75**, R43–R49.
13 T. Sreeprasad, M. S. Maliyekkal, K. Deepti, K. Chaudhari, P. L. Xavier and T. Pradeep, *ACS Appl. Mater. Interfaces*, 2011, **3**, 2643–2654.
14 B. Lu, T. Li, H. Zhao, X. Li, C. Gao, S. Zhang and E. Xie, *Nanoscale*, 2012, **4**, 2978–2982.
15 O. Akhavan, E. Ghaderi and A. Esfandiar, *J. Phys. Chem. B*, 2011, **115**, 6279–6288.
16 B. Baker, P. Zambryski, B. Staskawicz and S. Dinesh-Kumar, *Science*, 1997, **276**, 726–733.
17 M. McMullen, R. Jones and D. Gallenberg, *Plant Dis.*, 1997, **81**, 1340–1348.
18 M. L. Cohen, *Science*, 1992, **257**, 1050–1055.
19 F. Rezzonico, V. O. Stockwell and B. Duffy, *Antimicrob. Agents Chemother.*, 2009, **53**, 3173–3177.
20 P. Setlow, *J. Appl. Microbiol.*, 2006, **101**, 514–525.
21 J. H. Jung, D. S. Cheon, F. Liu, K. B. Lee and T. S. Seo, *Angew. Chem., Int. Ed.*, 2010, **49**, 5708–5711.
22 A. Teich and J. Hamilton, *Appl. Environ. Microbiol.*, 1985, **49**, 1429–1431.
23 Y. Sugiura, K. Fukasaku, T. Tanaka, Y. Matsui and Y. Ueno, *Appl. Environ. Microbiol.*, 1993, **59**, 3334–3338.
24 M. Boosalis, *Phytopathology*, 1952, **42**, 387–395.
25 P. B. Lindgren, R. C. Peet and N. J. Panopoulos, *J. Bacteriol.*, 1986, **168**, 512–522.
26 W. S. Hummers Jr and R. E. Offeman, *J. Am. Chem. Soc.*, 1958, **80**, 1339.

27 K. Y. Seong, X. Zhao, J. R. Xu, U. Güldener and H. C. Kistler, *Fungal Genet. Biol.*, 2008, **45**, 389–399.
28 S. Kang, M. Pinault, L. D. Pfefferle and M. Elimelech, *Langmuir*, 2007, **23**, 8670–8673.
29 H. M. Shapiro, P. J. Natale and L. A. Kamentsky, *Proc. Natl. Acad. Sci. U. S. A.*, 1979, **76**, 5728–5730.
30 D. Novo, N. G. Perlmutter, R. H. Hunt and H. M. Shapiro, *Cytometry*, 1999, **35**, 55–63.
31 C. C. Steel and R. B. Drysdale, *Phytochemistry*, 1988, **27**, 1025–1030.
32 P. Setlow, *Curr. Opin. Microbiol.*, 2003, **6**, 550–556.
33 S. D. Harris, *Mycologia*, 2005, **97**, 880–887.
34 P. Dimroth, *Biochim. Biophys. Acta, Bioenerg.*, 2000, **1458**, 374–386.
35 N. Charon, E. Greenberg, M. Koopman and R. Limberger, *Res. Microbiol.*, 1992, **143**, 597–603.
36 J. B. Russell, *Appl. Environ. Microb.*, 1990, **56**, 3304–3307.
37 D. Y. Lyon and P. J. Alvarez, *Environ. Sci. Technol.*, 2008, **42**, 8127–8132.
38 H. Q. Chen, B. W. Wang, D. Gao, M. Guan, L. N. Zheng, H. Ouyang, Z. F. Chai, Y. L. Zhao and W. Y. Feng, *Small*, 2013, **9**, 2735–2746.
39 X. Li, Y. Shi, B. Miao and Y. Zhao, *J. Phys. Chem. B*, 2012, **116**, 5391–5397.
40 Y. Li and N. Gu, *J. Phys. Chem. B*, 2010, **114**, 2749–2754.
41 J. Katoch, S. N. Kim, Z. Kuang, B. L. Farmer, R. R. Naik, S. A. Tatulian and M. Ishigami, *Nano Lett.*, 2012, **12**, 2342–2346.
42 W. Qin, X. Li, W. W. Bian, X. J. Fan and J. Y. Qi, *Biomaterials*, 2010, **31**, 1007–1016.
43 H. Z. Lei, L. J. Mi, X. J. Zhou, J. J. Chen, J. Hu, S. W. Guo and Y. Zhang, *Nanoscale*, 2011, **3**, 3888–3892.
44 C. Rajesh, C. Majumder, H. Mizuseki and Y. Kawazoe, *J. Chem. Phys.*, 2009, **130**, 124911.
45 J. S. Kim, E. Kuk, K. N. Yu, J.-H. Kim, S. J. Park, H. J. Lee, S. H. Kim, Y. K. Park, Y. H. Park and C.-Y. Hwang, *Nanomed.: Nanotechnol., Biol. Med.*, 2007, **3**, 95–101.
46 S. J. Lin, J. Reppert, Q. Hu, J. S. Hudson, M. L. Reid, T. A. Ratnikova, A. M. Rao, H. Luo and P. C. Ke, *Small*, 2009, 1128–1132.
47 Y. L. Chang, S.-T. Yang, J.-H. Liu, E. Dong, Y. W. Wang, A. Cao, Y. F. Liu and H. F. Wang, *Toxicol. Lett.*, 2011, **200**, 201–210.
48 M. Paidhungat and P. Setlow, *Bacillus subtilis and its relatives: from genes to cells*, American Society for Microbiology, Washington, DC, 2002, pp. 537–548.
49 A. V. Titov, P. Král and R. Pearson, *ACS Nano*, 2009, **4**, 229–234.
50 I. D. Iliev, V. A. Funari, K. D. Taylor, Q. Nguyen, C. N. Reyes, S. P. Strom, J. Brown, C. A. Becker, P. R. Fleshner and M. Dubinsky, *Science*, 2012, **336**, 1314–1317.
51 R. Tennen, B. Setlow, K. L. Davis, C. A. Loshon and P. Setlow, *J. Appl. Microbiol.*, 2000, **89**, 330–338.